DOI: 10.1002/chem.201000327

Gold Sulfide Nanoclusters: A Unique Core-In-Cage Structure

De-en Jiang,*[a] Michael Walter,[b, c] and Sheng Dai[a]

Nanoparticles of chalcogenides of group 12 elements, such as CdS, ignited a revolution in nanoscience.[1] These quantum dots have the bulk bonding structure and a larger tunable optical gap than the bulk, and find wide applications in biomedical imaging,[2] electronic devices,[3] and solar cells.[4] However, few studies have been directed toward the nanoparticles of Au chalcogenides, such as Au_2S. Although nanocrystals of Cu_2S and Ag_2S have recently been synthesized in a controllable way,[5] wet-chemistry preparation of Au_2S nanoparticles by reduction of Au^{III} often led to a mixture that contained Au nanoparticles.[6] Typical sizes of prepared Au_2S nanoparticles range from 4 to 7 nm. Little is known of Au_2S nanoparticles below 4 nm.

In contrast, monodisperse thiolated gold nanoparticles can be made in a variety of sizes, from sub-nanometer to several nanometers;[7] in fact, $Au_{102}(SR)_{44}$ and $Au_{25}(SR)_{18}^-$ have been crystallized (SR = thiolate group).[8] The Au–S framework of $Au_{25}(SR)_{18}^-$ is about 1 nm in size. Jin and coworkers[9] found that when the $Au_{25}(SR)_{18}^-$ clusters are subjected to in-source fragmentation in matrix-assisted laser desorption/ionization (MALDI) mass spectrometry, a series of $Au_xS_y^-$ clusters are recorded in the mass spectrum due to selective breaking of the S–C bonds[10] and loss of all R groups and some S atoms. The most abundant species is $Au_{25}S_{12}^-$, followed by $Au_{23}S_{11}^-$ and $Au_{27}S_{13}^-$. $Au_{25}S_{12}^-$ can also lose a single Au atom to give $Au_{24}S_{12}^-$.[9] The abundance of $Au_{25}S_{12}^-$ is independent of the RS group,[9] which indicates that this cluster has some magic nature. Because these $Au_xS_y^-$ clusters have an Au/S ratio of close to 2, they provide a means to fill our knowledge gap regarding Au_2S nanoclusters in this size range.

To understand these $Au_xS_y^-$ clusters, one needs to discover their structures. However, the only available experimental data are the mass spectra.[9] Given the absence of knowledge, a global minimum search is needed to elucidate these $Au_xS_y^-$ clusters. To that end, we have employed the basin-hopping technique[11] for a global minimum search with geometry optimization by density functional theory (see the Computational Methods section and the Supporting Information for details). This DFT-based basin-hopping is a powerful tool for finding global minima for clusters in which classical potentials are either unavailable or not accurate enough to be predictive; it has been successfully employed for many systems, such as gold, silicon, and carbon–boron clusters.[12] Herein, we used this technique and found global minima for the three most abundant $Au_xS_y^-$ clusters; a structural pattern emerges that indicates these clusters are symmetric with a unique core-in-cage construction, which can explain the observed mass peaks.[9]

Our approach to finding the global minima of $Au_xS_y^-$ followed the history of the sample in the MALDI experiment. We started with the structure of the $Au_{25}(SR)_{18}^-$ cluster with 18 R groups removed (Figure 1a). We then assumed that the middle S atoms of the six S-Au-S-Au-S motifs are lost (Figure 1b);[9b] this is a convenient assumption in that these six S atoms belong to the same group (roughly equivalent in symmetry) and are 1.1 Å farther from the cluster center than the other 12 S atoms. We then performed a geometry optimization of the $Au_{25}S_{12}^-$ structure in Figure 1b and obtained a local minimum (Figure 1c). The structural change from Figure 1b to c is rather dramatic and is accompanied by a huge lowering in energy (1785.0 kJ mol^{-1}); the local minimum is a distorted structure with two $(AuS)_3$ triangular rings and a longer Au–S oligomer on the cluster surface.

Starting with Figure 1c as our initial guess, we performed a DFT-based basin-hopping search for the global minimum. After about 600 Monte-Carlo steps, we found the highly

[a] Dr. D.-e. Jiang, Dr. S. Dai
Chemical Sciences Division,
Oak Ridge National Laboratory
Oak Ridge, TN, 37831 (USA)
Fax: (+1) 865-576-5235
E-mail: jiangd@ornl.gov

[b] Dr. M. Walter
Physics Department, University of Freiburg
Hermann-Herder-Strasse 3
79106 Freiburg (Germany)

[c] Dr. M. Walter
Freiburg Materials Research Center, University of Freiburg
Stefan-Meier-Strasse 21
79104 Freiburg (Germany)

Supporting information for this article is available on the WWW under http://dx.doi.org/10.1002/chem.201000327.

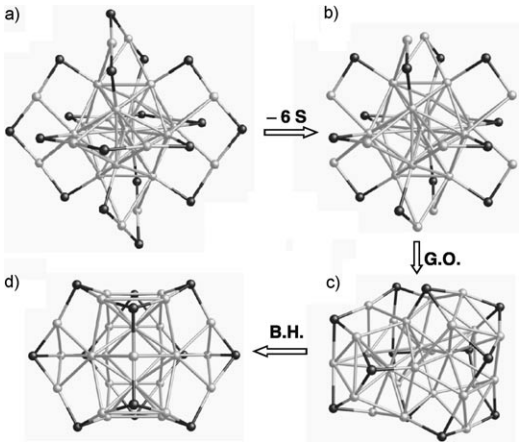

Figure 1. Evolution of the structure for $Au_{25}S_{12}^-$: a) The Au–S framework of $Au_{25}(SR)_{18}^-$; b) removal of six middle S atoms from the S-Au-S-Au-S motifs; c) a local minimum obtained by geometry optimization (G.O.) of b); d) global minimum found by DFT-based basin-hopping (B.H.) starting from c). Au: light grey; S: black.

symmetric structure in Figure 1d which is 212.3 kJ mol^{-1} lower in energy than Figure 1c. We consider this structure as the putative global minimum for $Au_{25}S_{12}^-$ because 600 additional Monte-Carlo steps did not give any lower-energy structure. The relatively small energy difference between Figure 1c and d (212.3 kJ mol^{-1}) compared with that between Figure 1b and c indicates that Figure 1c is a good initial guess that already has some features of the found global minimum. In other words, our approach of following the sample history during experiments worked.

The putative global minimum we found for $Au_{25}S_{12}^-$ features a unique core-in-cage construction (Figure 2). The

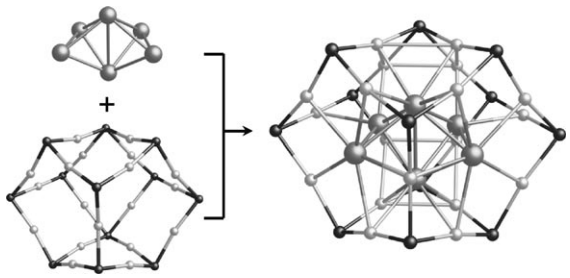

Figure 2. Dissecting the structure of $Au_{25}S_{12}^-$, a bi-tetrahedral Au_6 core inside an $Au_{19}S_{12}$ cage. The structure on the right is the same as in Figures 1d and 4b. S: black; Au in cage: light grey; Au in core: large gray spheres.

cage is formed with 12 S atoms as the vertices and 19 Au atoms at the midpoints of the edges connecting the vertices with Au–S bonds of 2.40 ± 0.05 Å in length. Therefore, the cage is well defined and tiled with two pentagons and seven quadrilaterals. The Au–S interaction in the cage is predominately covalent, as evidenced by the distribution of electron density that shows significant overlap in the middle of the Au–S bond (see Figure S1 in the Supporting Information). The core, or what remains when the cage is removed from the structure, is an edge-sharing bi-tetrahedral Au_6 (Figure 2). When the core is put inside the cage, the two far-apart Au atoms stick into the centers of the two pentagon windows of the cage; the remaining four gold atoms of the core stay inside the cage (Figure 2). The gold-gold interactions between the core and cage Au atoms and among the cage Au atoms themselves, as evidenced by the short distances (2.9~3.1 Å), are aurophilic[13] in nature and contribute to the overall stability of the cluster. There is no direct interaction between the core Au atoms and the S atoms on the cage (minimum distance at 3.5 Å).

The core-in-cage structure we found for $Au_{25}S_{12}^-$ is distinct from bulk Au_2S in that the cluster has a metallic core, whereas the bulk, which has the cuprite (C_3) structure, consists of two interpenetrating, weakly interacting cristobalite-like Au_2S networks (see Figure S2 in the Supporting Information). The pentagons and quadrilaterals forming the cage of $Au_{25}S_{12}^-$ are completely absent in bulk Au_2S, which exclusively consists of hexagonal rings. In bulk Au_2S, each Au atom is linearly coordinated by two S atoms and each S is tetrahedrally coordinated by four Au atoms, whereas the S atoms on the cage of $Au_{25}S_{12}^-$ are mainly coordinated by three Au atoms. This decreased coordination number for S but not Au in the cage indicates that the Au/S ratio on the cage is close to 1.5, similarly to the thioaruate(I) anion $[Au_{12}S_8]^{4-}$.[14] Therefore, more Au atoms are needed inside the cage to achieve the desired stoichiometry of 2, and the resultant additional Au–Au interaction between the core and the cage also stabilizes the cluster. Our charge analysis shows that the Au_6 core has a total charge of +0.6 e, which indicates that the electrostatic attraction between the core and the cage also plays a role.

The core-in-cage structure we found for $Au_{25}S_{12}^-$ can also explain the observed mass peak for $Au_{24}S_{12}^-$.[9] Due to the large windows of the cage, the core Au atoms (especially the two at the pentagon centers, Figure 2) can be lost one at a time with minimal change to the cage structure. We confirmed that it does indeed take less energy to remove one core Au atom (from the pentagon center) than one on the cage.

To test stability and dynamics of the core-in-cage structure of $Au_{25}S_{12}^-$, we performed simulated annealing with DFT-based molecular dynamics by heating up the cluster and equilibrating at 1000 K for 10 ps before cooling down to 0 K. We found that the core-in-cage feature survived this process despite the dynamic rearrangement of the cage. Finally, a new local minimum (Figure 3) that is 84.9 kJ mol^{-1} higher in energy than the global minimum was found. Interestingly, this new local minimum features a triangle on the cage, similar to that in Figure 1c. The fact that no lower-energy structure was found in the simulated annealing process further indicates that the putative global minimum we found for $Au_{25}S_{12}^-$ may indeed be the true one.

We now turn to the next two most abundant clusters, $Au_{23}S_{11}^-$ and $Au_{27}S_{13}^-$. For $Au_{23}S_{11}^-$, we removed two Au atoms and one S atom from the global minimum of

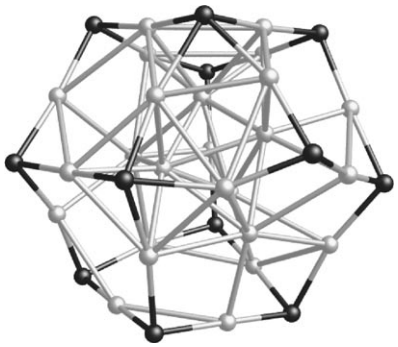

Figure 3. A local minimum found for $Au_{25}S_{12}^-$ by annealing the global minimum (Figure 1d) at 1000 K for 10 ps. Au: light gray; S: black.

$Au_{25}S_{12}^-$, then performed the DFT-based basin-hopping search. The obtained global minimum is also a symmetric core-in-cage structure (Figure 4a). Now the 11 S vertices are connected by 17 Au edges and tiled with two pentagons and six quadrilaterals; the core still has six Au atoms that form an oblique triangular prism (Figure 5). The initial structure of $Au_{27}S_{13}^-$ is built upon the $Au_{25}S_{12}^-$ structure by adding one S vertex and one Au edge to the cage and another Au atom to the core. Then a DFT-based basin-hopping was performed. The global minimum found has four pentagons and five quadrilaterals tiling the cage (Figure 4c); the Au_7 core forms an approximately pentagonal bipyramid (Figure 6).

We compare the properties of $Au_{23}S_{11}^-$, $Au_{25}S_{12}^-$, and $Au_{27}S_{13}^-$ in Table 1. The computed HOMO–LUMO gap decreases slightly from 1.2 eV for $Au_{23}S_{11}^-$ to 0.93 eV for $Au_{27}S_{13}^-$. We note that bulk Au_2S has a much higher computed band gap (2.3 eV), which indicates that the metallic gold core in the $Au_xS_y^-$ clusters lead to a lower HOMO–LUMO gap. The superatom complex (SAC) concept has been successfully used to explain the electronic structure of thiolated gold nanoclusters.[15] Herein, we apply the same concept to $Au_xS_y^-$ clusters that are derived from thiolated gold clusters. According to the SAC concept, the delocalized electrons of the whole cluster occupy the superatomic orbitals in the following order: 1S, 1P, 1D, and so forth. To count the delocalized electrons in $Au_xS_y^-$ clusters, we assumed that each Au atom contributes one valence electrons whereas S has a formal oxidation state of −2, thereby localizing two electrons. So all three $Au_xS_y^-$ clusters ($Au_{23}S_{11}^-$, $Au_{25}S_{12}^-$, and $Au_{27}S_{13}^-$) have two delocalized electrons that occupy the 1S orbital, leaving 1P empty. The same electron count indicates similar electronic structures among the three clusters, which agrees

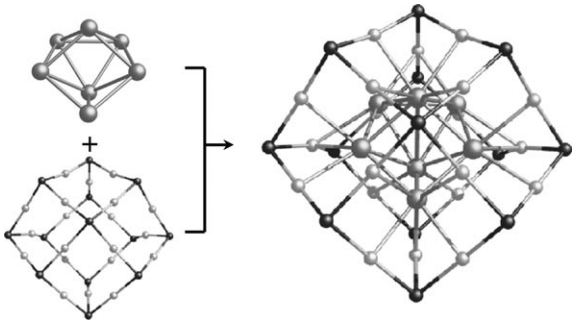

Figure 6. Dissecting the structure of $Au_{27}S_{13}^-$, an approximately pentagonal bipyramid Au_7 core inside an $Au_{20}S_{13}$ cage. The structure on the right is the same as in Figure 4c. S: black; Au in cage: light grey; Au in core: large grey spheres.

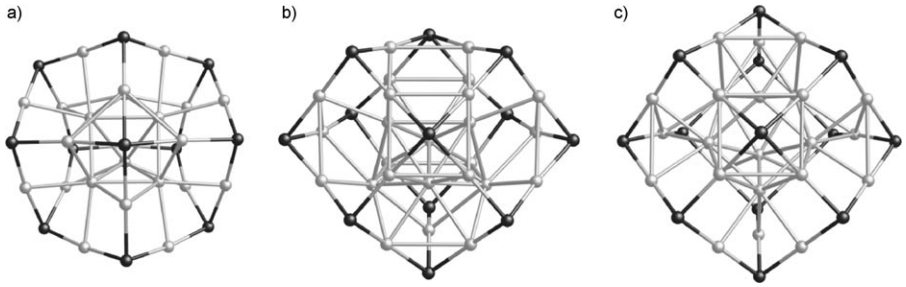

Figure 4. Global minima for a) $Au_{23}S_{11}^-$, b) $Au_{25}S_{12}^-$, and c) $Au_{27}S_{13}^-$. Au: light gray; S: black.

Table 1. HOMO–LUMO gap (HL gap), formation energy (ΔE_f),[a] adiabatic electron affinity (AEA), and adiabatic ionization potential (AIP) of $Au_{23}S_{11}^-$, $Au_{25}S_{12}^-$, and $Au_{27}S_{13}^-$.

Cluster	$Au_{23}S_{11}^-$	$Au_{25}S_{12}^-$	$Au_{27}S_{13}^-$
HL gap [eV]	1.20	1.08	0.93
ΔE_f [kJ mol^{-1}]	−293.4	−295.1	−293.6
AEA [eV]	0.91	1.02	1.42
AIP [eV]	4.80	4.70	4.70

[a] $\Delta E_f = [E(Au_xS_y^-) - xE(Au) - yE(S)]/(x+y)$, in which $E(Au_xS_y^-)$, $E(Au)$ and $E(S)$ are the energies of the cluster, Au atoms, and S atoms, respectively. 1 eV = 96.485 kJ mol^{-1}.

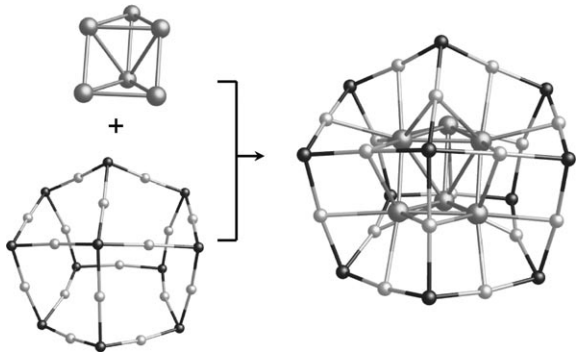

Figure 5. Dissecting the structure of $Au_{23}S_{11}^-$, an oblique triangular prism Au_6 core inside an $Au_{17}S_{11}$ cage. The structure on the right is the same as in Figure 4a. S: black; Au in cage: light grey; Au in core: large grey spheres.

with their similar HOMO–LUMO gaps. Using $Au_{25}S_{12}^-$ as an example, we examine its frontier orbitals in detail. Unlike thiolated gold clusters in which the HOMO is usually dominated by the delocalized superatomic orbitals,[16] we found that the HOMO of $Au_{25}S_{12}^-$ is dominated by localized bonding on the cage and the occupied 1S level (Figure 7, left) is shifted by 0.33 eV below the HOMO level. However, the LUMO of $Au_{25}S_{12}^-$ does indeed shows delocalized P-orbital character (Figure 7, right).

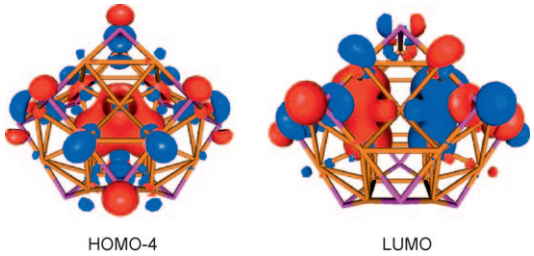

Figure 7. HOMO−4 and LUMO of $Au_{25}S_{12}^-$ that show the characters of delocalized 1S and 1P superatomic orbitals, respectively.

The computed formation energy shows that $Au_{25}S_{12}^-$ is slightly more stable than $Au_{23}S_{11}^-$ and $Au_{27}S_{13}^-$, which agrees well with the observed relative abundances of the three clusters.[9] We note that this agreement could be fortuitous given that the energy differences as computed in Table 1 are relatively small. However, the superior stability of $Au_{25}S_{12}^-$ does seem to have a structural origin; its core fits better inside the cage than the other two clusters. The computed adiabatic electron affinities and ionization potentials show that these three clusters are happy in their anion state, gaining little energy to become a dianion and requiring about 5 eV to lose an electron.

We believe that the core-in-cage structure is a rather general feature of gold sulfide nanoclusters at $\approx$1 nm. This insight has implications for synthesis of gold sulfide nanoparticles in this size range, for example, by reducing Au^{III} with Na_2S.[6] Moreover, the Au core inside the cage may catalyze reactions for small gas molecules that can access the core through the cage windows. Therefore, Au_2S clusters supported on porous oxides or embedded in a polymer matrix may have unique catalytic properties.

Herein, the basin-hopping search for the global minima was enabled by DFT-based geometry optimization. It is now a well-established fact that commonly used exchange-correlation functionals may give systematic errors for organic reactions involving carbon–carbon bond formation[17] and for isomerization energetics of alkanes.[18] Therefore, it is necessary to validate the DFT exchange-correlation functional used and explore multiple DFT models.[17] We used the Perdew–Burke–Erzonhoff (PBE) form[19] of the generalized-gradient approximation (GGA) for electron exchange and correlation when performing the basin-hopping search in this work. The PBE functional is one of the most popular choices among many GGA functionals and a great many successful examples are reported in the literature. More relevantly, the PBE functional has been successfully used to explore and especially predict thiolated gold nanoclusters,[15,20] including the basin-hopping search based on DFT-PBE geometry optimization.[18g] These successes lend confidence to our present exploration of $Au_xS_y^-$ clusters with DFT-PBE geometry optimization.

However, it has been shown that the PBE functional overestimates the lattice parameters for many semiconductors,[21] including Au_2S, and that *meta*-GGA functionals, such as the non-empirical Tao–Perdew–Staroverov–Scuseria (TPSS) functional,[22] can describe the aurophilic interactions in gold clusters and gold complexes better than the local density approximation, GGA, and hybrid functionals.[23] Therefore, we examined several distinct lowest-energy configurations from the basin-hopping search, including the global minimum, and optimized the structures with both PBE and TPSS functionals (Figure S4 in the Supporting Information). We found that the global minimum from the PBE functional is also the global minimum for the TPSS functional. More recently, it has been shown[24] that the M06L *meta*-GGA functional[25] can correctly predict the critical sizes of 2D–3D transitions for cationic and anionic gold clusters based on the PBE-optimized geometries, so we also compared the PBE, TPSS, and M06L functionals together for several configurations along the basin-hopping search path based on the PBE-optimized geometries. The results are shown in Figure S5 in the Supporting Information; it can be seen that the trends of relative energies are basically the same for the three functionals (except for one point at about the 200th step at which M06L differs from PBE and TPSS) and that the global minimum we found from the DFT-PBE basin-hopping is also the lowest-energy configuration for TPSS and M06L. Because the nonempirical nature of the TPSS functional appeals to us, the results are reported in this paper for the TPSS functional. These further checks validate to a large degree our approach of basin-hopping by DFT-PBE geometry optimization of $Au_xS_y^-$ clusters with final refinement by using the TPSS functional.

In summary, we found a symmetric core-in-cage structure for the most abundant gold sulfide nanoclusters observed in MALDI fragmentation of $Au_{25}(SR)_{18}^-$ by using a DFT-based basin-hopping global-minimum search. S atoms form the vertices of the cage and are connected by the Au atoms at the edges, whereas the rest of the Au atoms form a metallic core inside the cage. This core-in-cage structure is distinct from bulk gold sulfide. Our work herein fills the knowledge gap regarding the structure of gold sulfide nanoclusters at $\approx$1 nm and stimulates more experiments of nanostructures of gold chalcogenides at this size range.

Computational Methods

The global minimum search was performed by using a Python script (available upon request) to interface the basin-hopping algorithm[11] with the Vienna Ab Initio Simulation Package (VASP)[26] for density function-

al theory geometry optimization. The Perdew–Burke–Erzonhoff (PBE) form of the generalized-gradient approximation (GGA) was chosen for electron exchange and correlation,[19] and the electron-core interaction was described by the projector-augmented wave (PAW) method within the frozen-core approximation.[27] The global minimum found by VASP basin-hopping was then re-optimized with Turbomole V5.10, which was used for parallel resolution-of-identity density functional theory (RI-DFT) calculations.[28] The def2-TZVP orbital and auxiliary basis sets[29] were used for all atoms for structural optimization. Effective core potentials that have 19 valence electrons and include scalar relativistic corrections were used for Au.[30] Comparisons between PBE, TPSS, and M06L functionals were done by employing the grid-projector-augmented-wave (GPAW) method.[31] See the Supporting Information for more details.

Acknowledgements

This work was supported by the Division of Chemical Sciences, Geosciences, and Biosciences, Office of Basic Energy Sciences, U.S. Department of Energy under contract no. DE-AC05-00OR22725 with UT-Battelle, LLC. D.E.J. thanks Drs. R. C. Jin, Z. K. Wu, and P. R. Kent for helpful discussions. We also thank an anonymous reviewer for the comments that have greatly improved this paper. This research used resources of the National Energy Research Scientific Computing Center, which is supported by the Office of Science of the U.S. Department of Energy under contract no. DE-AC02-05CH11231.

Keywords: basin-hopping · cluster compounds · density functional calculations · global minima · gold sulfides

[1] A. P. Alivisatos, *Science* **1996**, *271*, 933.
[2] M. Bruchez, Jr., M. Moronne, P. Gin, S. Weiss, A. P. Alivisatos, *Science* **1998**, *281*, 2013.
[3] V. L. Colvin, M. C. Schlamp, A. P. Alivisatos, *Nature* **1994**, *370*, 354.
[4] a) J. H. Bang, P. V. Kamat, *ACS Nano* **2009**, *3*, 1467; b) B. Farrow, P. V. Kamat, *J. Am. Chem. Soc.* **2009**, *131*, 11124; c) P. V. Kamat, G. C. Schatz, *J. Phys. Chem. C* **2009**, *113*, 15473.
[5] a) F. Gao, Q. Y. Lu, D. Y. Zhao, *Nano Lett.* **2003**, *3*, 85; b) K. Jang, S. Y. Kim, K. H. Park, E. Jang, S. Jun, S. U. Son, *Chem. Commun.* **2007**, 4474; c) D. S. Wang, T. Xie, Q. Peng, Y. D. Li, *J. Am. Chem. Soc.* **2008**, *130*, 4016; d) Z. B. Zhuang, Q. Peng, B. Zhang, Y. D. Li, *J. Am. Chem. Soc.* **2008**, *130*, 10482.
[6] a) T. Morris, H. Copeland, G. Szulczewski, *Langmuir* **2002**, *18*, 535; b) K. Yoshizawa, K. Iwahori, K. Sugimoto, I. Yamashita, *Chem. Lett.* **2006**, *35*, 1192; c) A. M. Schwartzberg, C. D. Grant, T. van Buuren, J. Z. Zhang, *J. Phys. Chem. C* **2007**, *111*, 8892; d) C. L. Kuo, M. H. Huang, *J. Phys. Chem. C* **2008**, *112*, 11661; e) Y. Mikhlin, M. Likhatski, A. Karacharov, V. Zaikovski, A. Krylov, *Phys. Chem. Chem. Phys.* **2009**, *11*, 5445.
[7] a) M. Brust, M. Walker, D. Bethell, D. J. Schiffrin, R. Whyman, *J. Chem. Soc. Chem. Commun.* **1994**, 801; b) T. G. Schaaff, M. N. Shafigullin, J. T. Khoury, I. Vezmar, R. L. Whetten, W. G. Cullen, P. N. First, C. Gutierrez Wing, J. Ascensio, M. J. Jose Yacaman, *J. Phys. Chem. B* **1997**, *101*, 7885; c) T. G. Schaaff, R. L. Whetten, *J. Phys. Chem. B* **2000**, *104*, 2630; d) Y. Negishi, K. Nobusada, T. Tsukuda, *J. Am. Chem. Soc.* **2005**, *127*, 5261.
[8] a) P. D. Jadzinsky, G. Calero, C. J. Ackerson, D. A. Bushnell, R. D. Kornberg, *Science* **2007**, *318*, 430; b) M. W. Heaven, A. Dass, P. S. White, K. M. Holt, R. W. Murray, *J. Am. Chem. Soc.* **2008**, *130*, 3754; c) M. Zhu, C. M. Aikens, F. J. Hollander, G. C. Schatz, R. Jin, *J. Am. Chem. Soc.* **2008**, *130*, 5883.
[9] a) M. Zhu, E. Lanni, N. Garg, M. E. Bier, R. Jin, *J. Am. Chem. Soc.* **2008**, *130*, 1138; b) Z. K. Wu, C. Gayathri, R. R. Gil, R. C. Jin, *J. Am. Chem. Soc.* **2009**, *131*, 6535; c) Z. K. Wu, R. C. Jin, *ACS Nano* **2009**, *3*, 2036.
[10] a) R. J. Arnold, J. P. Reilly, *J. Am. Chem. Soc.* **1998**, *120*, 1528; b) Y. Negishi, T. Tsukuda, *J. Am. Chem. Soc.* **2003**, *125*, 4046.
[11] D. J. Wales, J. P. K. Doye, *J. Phys. Chem. A* **1997**, *101*, 5111.
[12] a) S. Yoo, J. J. Zhao, J. L. Wang, X. C. Zeng, *J. Am. Chem. Soc.* **2004**, *126*, 13845; b) E. Aprà, R. Ferrando, A. Fortunelli, *Phys. Rev. B* **2006**, *73*, 205414; c) S. Bulusu, X. C. Zeng, *J. Chem. Phys.* **2006**, *125*, 154303; d) Y. Pei, X. C. Zeng, *J. Am. Chem. Soc.* **2008**, *130*, 2580.
[13] P. Pyykkö, *Angew. Chem.* **2004**, *116*, 4512; *Angew. Chem. Int. Ed.* **2004**, *43*, 4412.
[14] G. Marbach, J. Strähle, *Angew. Chem.* **1984**, *96*, 695; *Angew. Chem. Int. Ed. Engl.* **1984**, *23*, 715.
[15] M. Walter, J. Akola, O. Lopez-Acevedo, P. D. Jadzinsky, G. Calero, C. J. Ackerson, R. L. Whetten, H. Gönbeck, H. Häkkinen, *Proc. Natl. Acad. Sci. USA* **2008**, *105*, 9157.
[16] D. E. Jiang, R. L. Whetten, W. D. Luo, S. Dai, *J. Phys. Chem. C* **2009**, *113*, 17291.
[17] C. E. Check, T. M. Gilbert, *J. Org. Chem.* **2005**, *70*, 9828.
[18] a) S. Grimme, *Angew. Chem.* **2006**, *118*, 4571; *Angew. Chem. Int. Ed.* **2006**, *45*, 4460; b) M. D. Wodrich, C. Corminboeuf, P. von R. Schleyer, *Org. Lett.* **2006**, *8*, 3631.
[19] J. P. Perdew, K. Burke, M. Ernzerhof, *Phys. Rev. Lett.* **1996**, *77*, 3865.
[20] a) J. Akola, M. Walter, R. L. Whetten, H. Häkkinen, H. Grönbeck, *J. Am. Chem. Soc.* **2008**, *130*, 3756; b) D. E. Jiang, M. L. Tiago, W. D. Luo, S. Dai, *J. Am. Chem. Soc.* **2008**, *130*, 2777; c) D. E. Jiang, W. Luo, M. L. Tiago, S. Dai, *J. Phys. Chem. C* **2008**, *112*, 13905; d) Y. Pei, Y. Gao, X. C. Zeng, *J. Am. Chem. Soc.* **2008**, *130*, 7830; e) O. Lopez-Acevedo, J. Akola, R. L. Whetten, H. Grönbeck, H. Häkkinen, *J. Phys. Chem. C* **2009**, *113*, 5035; f) Y. Pei, Y. Gao, N. Shao, X. C. Zeng, *J. Am. Chem. Soc.* **2009**, *131*, 13619.
[21] J. Heyd, J. E. Peralta, G. E. Scuseria, R. L. Martin, *J. Chem. Phys.* **2005**, *123*, 174101.
[22] J. M. Tao, J. P. Perdew, V. N. Staroverov, G. E. Scuseria, *Phys. Rev. Lett.* **2003**, *91*, 146401.
[23] M. P. Johansson, A. Lechtken, D. Schooss, M. M. Kappes, F. Furche, *Phys. Rev. A* **2008**, *77*, 053202.
[24] L. Ferrighi, B. Hammer, G. K. H. Madsen, *J. Am. Chem. Soc.* **2009**, *131*, 10605.
[25] Y. Zhao, D. G. Truhlar, *J. Chem. Phys.* **2006**, *125*, 194101.
[26] a) G. Kresse, J. Furthmüller, *Comput. Mater. Sci.* **1996**, *6*, 15; b) G. Kresse, J. Furthmüller, *Phys. Rev. B* **1996**, *54*, 11169.
[27] a) P. E. Blöchl, *Phys. Rev. B* **1994**, *50*, 17953; b) G. Kresse, D. Joubert, *Phys. Rev. B* **1999**, *59*, 1758.
[28] R. Ahlrichs, M. Bar, M. Haser, H. Horn, C. Kolmel, *Chem. Phys. Lett.* **1989**, *162*, 165.
[29] F. Weigend, M. Haser, H. Patzelt, R. Ahlrichs, *Chem. Phys. Lett.* **1998**, *294*, 143.
[30] D. Andrae, U. Haussermann, M. Dolg, H. Stoll, H. Preuss, *Theor. Chim. Acta* **1990**, *77*, 123.
[31] a) J. J. Mortensen, L. B. Hansen, K. W. Jacobsen, *Phys. Rev. B* **2005**, *71*, 035109; b) GPAW is freely available under https://wiki.fysik.dtu.dk/gpaw.

Received: February 6, 2010
Published online: March 26, 2010

